Phyton-
International Journal of
Experimental Botany

Tech Science Press

http://doi.org/10.32604/phyton.2026.084714

ARTICLE

Antifungal Activity and Mechanistic Insights of Clove Essential Oil Against *Fusarium oxysporum*-Induced Root Rot Disease via Molecular Docking of Its Major Components

Hualin Hu[1,2,*], Caiwei Wang[1,2], Jian Fan[1,2], Chengmei Wang[3] and Chunguang Ren[4]

[1]Natural Products Research Center of Guizhou Province, Guiyang, China
[2]State Key Laboratory of Discovery and Utilization of Functional Components in Traditional Chinese Medicine, School of Pharmaceutical Sciences, Guizhou Medical University, Guiyang, China
[3]Forestry and Agricultural Service Center of Xinba Town, Guiding County, Qiannan, China
[4]Guizhou Institute of Mountain Resources, Guiyang, China
*Corresponding Author: Hualin Hu. Email: dewxfss0307@163.com

Received: 28 April 2026; Accepted: 28 July 2026; Published: 24 September 2026

ABSTRACT: Clove (*Syzygium aromaticum*), a member of the Myrtaceae family, is widely distributed throughout tropical regions from Indonesia to China. This research aimed to investigate the antifungal effects and mechanisms of clove essential oil (CEO) against *Fusarium oxysporum*, the causal agent of root rot disease in *Pseudostellaria heterophylla* and other crops. The inhibitory effects of CEO on mycelial growth, spore germination and ergosterol biosynthesis of *F. oxysporum* were assessed through *in vitro* assays. The mechanism was initially investigated by analyzing the primary components of CEO using gas chromatography-mass spectrometry (GC-MS) and performing molecular docking studies with the target enzyme. Results showed that CEO inhibited mycelial radial growth in a dose-dependent manner, with inhibition rates ranging from 16.61% to 100%. The median effective concentration (EC_{50}) value was determined to be 131.7 μL/L (R^2 = 0.985). Spore germination decreased significantly by 61.6% at 300 μL/L ($p < 0.05$), resulting in shortened germ tubes and noticeable morphological changes. CEO inhibited ergosterol biosynthesis in a concentration-dependent manner, disrupting membrane integrity. The inhibition rate can reach 34.6% at 150 μL/L ($p < 0.05$). GC-MS analysis identified 24 compounds, with phenylpropanoids representing 92.44% of compounds. Within this category, eugenol and eugenyl acetate were the predominant components, representing 72.51% and 19.66%, respectively. The molecular docking results showed that eugenyl acetate exhibits a strong binding affinity for ERG3 and CYP51, with binding free energies of −6.615 and −6.336 kcal/mol, respectively. This research identifies eugenyl acetate as a key component contributing to the antifungal effect through molecular docking, and reveals a dual-action antifungal mechanism of CEO against *F. oxysporum*. These findings suggest that CEO has potential natural antifungal agent for controlling soil-borne diseases by disrupting membranes through ergosterol inhibition.

KEYWORDS: *Syzygium aromaticum*; phenylpropanoids; morphological analysis; ergosterol biosynthesis; eugenyl acetate

1 Introduction

Root rot disease is a serious plant disease caused by soilborne fungi, such as *Fusarium oxysporum*, *Rhizoctonia solani*, and *Fusarium striatum*, among others [1–4]. It is characterized by root infections, vascular bundle lesions, hindered water and nutrient uptake, plant wilting, and ultimately plant demise [5–7]. These pathogens thrive in warm and humid conditions, spreading rapidly among key crops such as wheat, corn, soybeans, and tomatoes, resulting in substantial agricultural losses [8–12]. The Food and Agriculture

Organization of the United Nations (FAO) reports that plant diseases and pests lead to a global reduction in crop yields of up to 40% annually. Specifically, soybean losses alone exceed 10 million tons each year [13], directly resulting in approximately 1 to 2 billion US dollars in global economic losses annually [14].

Traditional chemical fungicides like triazoles and benzimidazoles can control root rot initially, but they can be dangerous in the long term because of resistance to fungicides. *Fusarium pseudograminearum*, wheat crown rot pathogen, has resistance to fludioxonil and tebuconazole in key wheat growing areas, so new fungicides with different action must be developed [15–18]. Excessive application of fungicides can lead to soil ecology disturbances, diminishing beneficial bacteria [19,20]. This disruption, as UNEP warned about global soil degradation, damages essential soil functions like cycling of nutrients, soil structure, and agroecosystem fertility [21,22]. Food safety concerns are caused by contamination of crops such as high residues of isoprothiolane and carbendazim in brown rice [23,24]. The increasing problem of pathogen resistance caused by long-term use of chemical disinfectants, coupled with escalating environmental pollution concerns, underscores the urgent need to adopt environmentally friendly and effective alternative management strategies.

Plant essential oils (EOs) have become promising alternatives to synthetic fungicides due to their broad antimicrobial activity, biodegradability, and low toxicity to mammals [25–29]. Among them, clove essential oil (CEO), rich in eugenol, has antifungal properties by breaking fungal cell membranes and causing reactive oxygen species production [30,31]. Despite increasing evidence that CEO possesses antifungal properties against various phytopathogens [32], its specific mode of action against *F. oxysporum* remains largely unclear. In particular, two critical knowledge gaps persist: (1) whether the observed growth inhibition is due to interference with ergosterol biosynthesis, a primary target of many antifungal agents, and (2) which specific components of CEO are responsible for this activity and how they interact with key enzymes in the ergosterol pathway at the molecular level. Traditional *in vitro* assays can quantify inhibitory effects, such as mycelial growth and spore germination, but they fail to elucidate molecular-scale interactions. To bridge this gap, molecular docking analysis is essential. This computational approach predicts and visualizes the binding affinities and interaction modes between CEO-derived compounds and target proteins, including lanosterol 14α-demethylase (CYP51) and C-5 sterol desaturase (ERG3). This analysis provides mechanistic insights that are not accessible through phenotyping alone.

Accordingly, we present an integrated, multi-scale study framework that connects phenotypic inhibition with molecular interactions: antifungal phenotyping measures inhibition of mycelial growth and spore germination by CEO via agar diffusion and liquid culture methods; biochemical analysis measures inhibition of ergosterol biosynthesis via saponification; GC-MS characterizes eugenol and eugenyl acetate as the primary bioactive parts of CEO and provides the foundation for molecular probe development. Molecular docking validation model binding of eugenol and eugenyl acetate to ergosterol targets (CYP51, ERG3) using AutoDock Vina provides mechanistic information about CEO antifungal properties. This study aimed to evaluate the antifungal activity of CEO against *F. oxysporum* and elucidate its mechanisms via inhibition of ergosterol biosynthesis, membrane disruption, and molecular docking for bioactive constituent identification – thereby establishing a mechanistic basis for plant pathogen control.

2 Materials and Methods

Plant materials and essential oil preparation: Clove buds were purchased from Tongjitang Pharmacy in Guiyang City, Guizhou Province, and originated from Guangxi. They were validated by Prof. Shaohuan Liu of Guizhou Medical University, and the voucher sample (DX20072905) was stored in the refrigerator of Laboratory A501 at −20°C. The CEO steam distillation method (with slight modifications

from Sarma et al [33]) used 300 g of clove buds hydrodistilled in a 5000 mL round-bottom flask connected to a Clevenger apparatus. Extraction was continued for 3 h at a 1:10 solid-to-solvent ratio (w/v) until clear distillate was obtained. The extraction was three technical replicates to obtain sufficient essential oil yield. The mixed distillate containing residual water was extracted in petroleum ether (40–60°C). The organic phase was isolated, concentrated using a rotary evaporator to remove solvent traces, and dried with anhydrous sodium sulfate. The extraction yield (%) was measured using Formula (1), and the obtained CEO was stored in sealed amber vials at 4°C until further analysis.

$$\text{Yield } (\%) = \frac{M_1}{M_2} \times 100\% \tag{1}$$

where M_1 is the mass of CEO (g) and M_2 is the mass of dried clove buds (g).

Strain reactivation and spore suspension preparation: The *F. oxysporum* isolate used in this study was obtained from Prof. Dan Zhou's research group at Guizhou Normal College and has been molecularly identified and characterized previously [34]. This isolate has not been deposited in any publicly accessible fungal culture collection; it is currently preserved in the −80°C ultra-low temperature freezer of Laboratory A501 and is available from the corresponding author upon reasonable request. For routine maintenance, the strain is subcultured on potato dextrose agar (PDA) slants and stored at 4°C for short-term use, while long-term storage is conducted in 20% (v/v) glycerol at −80°C. The isolate was retrieved from −80°C storage and reactivated through three consecutive subcultures on fresh PDA medium (Shanghai Bowei Biotechnology Co., Ltd., Shanghai, China) at 28 ± 1°C for 7 days, with the plates incubated in an inverted position. Upon reaching dense sporulation, mycelial plugs (7-mm diameter) were extracted from actively growing cultures using a cork borer and transferred to fresh PDA plates for further incubation at 28°C for 5 days. A spore suspension (1×10^6 CFU/mL) was prepared by filtration through sterile gauze, suspended in physiological saline, and stored at 4°C for future use.

Inhibitory effect of CEO on F. oxysporum mycelial growth: The antifungal efficacy of CEO against *F. oxysporum* was assessed using the poisoned food technique. Mycelial plugs (7 mm in diameter) from 5-day-old cultures were inoculated onto PDA plates (90 mm in diameter) supplemented with CEO at concentrations of 50, 100, 150, 200, 250, and 300 μL/L. Each Petri plate contained 20 mL of the amended medium. Control plates received no antifungal treatment. After an incubation period of 5 days at 28°C (with three biological replicates per treatment), colony diameters were measured along two perpendicular axes at randomly selected points on each colony. The percentage of inhibition in mycelial growth was computed using Formula (2). The median effective concentration (EC_{50}) value and the correlation coefficient (R^2) were ascertained through probit regression analysis.

$$\text{Mycelial growth inhibition } (\%) = \frac{D_c - D_t}{D_c} \times 100\% \tag{2}$$

where D_c represents the colony diameter in the control group (cm) and D_t denotes the colony diameter in the treated group (cm).

Effect of CEO on spore germination of F. oxysporum: Spore suspensions from 5-day-old PDA cultures were prepared by washing with sterile distilled water, followed by filtration. Aliquots (50 μL) of the suspension were then added to potato dextrose broth (PDB) with varying concentrations of CEO, followed by incubation at 28°C with shaking for 24 h. The spores, both germinated and ungerminated, were enumerated under a light microscope, with approximately 200 randomly sampled spores assessed per replicate across three independent biological replicate experiments. A spore was classified as germinated if

the length of its germ tube exceeded 50% of the spore diameter. The germination rate and inhibition rate (%) were computed using Formulas (3) and (4), respectively.

$$\text{Spore germination (\%)} = \frac{N_g}{N_t} \times 100\% \tag{3}$$

$$\text{Spore inhibition (\%)} = \frac{S_c - S_t}{S_c} \times 100\% \tag{4}$$

where N_g, N_t represents the number of germinated spores and spore count, respectively; S_c, S_t represents the germination rate in the control and treated group, respectively.

Assessment of the effect of CEO on ergosterol production: The determination of ergosterol content in *F. oxysporum* cell membranes was conducted using a saponification method [35,36]. Firstly, 0.0050 g of ergosterol standard substance was accurately weighed and promptly transferred to a 200 mL amber volumetric flask. It was dissolved in dichloromethane and then diluted to the mark with the same solvent to yield a 0.05 mg/mL stock solution. Subsequently, aliquots of 2.0, 4.0, 6.0, 8.0, and 10.0 mL were pipetted into separate 10 mL amber volumetric flasks and diluted to the mark to prepare standard solutions of 0.01, 0.02, 0.03, 0.04, and 0.05 mg/mL. All solutions were stored at 4°C. Secondly, Spore suspensions (5×10^5 CFU/mL) were inoculated into PDB medium with varying concentrations of CEO. Following a 5-day incubation period at 28°C with agitation, mycelia were harvested, washed twice with distilled water, and filtered through filter paper to maintain the original ergosterol levels in the cell membranes. Subsequently, each mycelial sample was treated with 4 mL of 25% NaOH-C_2H_5OH solution, vortexed for 5 min, and incubated at 85°C for 4 h. This was followed by the addition of 2 mL of sterile distilled water and 4 mL of dichloromethane, vortexed for 2 min, and the dichloromethane layer was collected to yield the test solution. The optical density (OD) of the resulting solution was measured at 284 nm using a UV/VIS spectrophotometer. Control samples, which were not exposed to CEO, were included for comparison. The ergosterol content was measured using three independent biological replicates and calculated according to Formula (5).

$$\text{Ergosterol content (\%)} = K \times \left(\frac{W \times V}{M} \right) \times 100\% \tag{5}$$

where K is the dilution factor, W is the ergosterol concentration determined from the standard curve (mg/mL), V is the volume of dichloromethane (mL), and M is the dry weight of mycelia (mg).

Morphological analysis of mycelia under CEO treatment: Aliquots (50 μL) of the suspension were transferred into PDB medium with different CEO concentrations (0, 100, 200, and 300 μL/L) and kept in the flasks at 28°C, then shaken at 150 rpm for 48 h. After the hyphae and spores were centrifuged at 5000 rpm for 10 min, washed twice with sterile distilled water, and the resultant pellet was oven-dried at 55°C to a constant weight. The samples were placed on glass slides and observed under an optical microscope (Phenix XSP-06, 1600× magnification). At least 10 random fields were imaged for each concentration. Micrographs were captured using an OPPO K11 camera, processed with ImageJ (v1.54f) for measurement, and scale bars were added based on calibration with a stage micrometer (10 μm per division).

GC-MS analysis: The CEO was randomly selected from one of the biological replicates, diluted to a 1:10 (v/v) ratio with n-hexane, and then subjected to gas chromatography-mass spectrometry (GC-MS) with 1 μL injection (split ratio 20:1). The separation was performed in a ZB-5MSI fused-silica capillary column (30 m × 0.25 mm × 0.25 μm film thickness) with a programmed temperature chain: initial temperature 48°C (held for 2 min), ramp 4°C/min to 206°C, then ramp 10°C/min to 310°C (held for 58 min). The injector

temperature was set at 250°C and helium carrier gas (99.999%) flowed consistently at 1 mL/min (with solvent delay 4.00 min). MS detection was electron impact ionization (70 eV) with the source at 230°C and the quadrupole at 150°C, scanning the m/z range of 29–500. Compound identification was performed using matching retention indexes and mass spectra (similarity >90%) with NIST 17/Wiley 275 libraries. To further confirm the identifications, Kovats retention indices (RI) were calculated for each compound using a homologous series of n-alkanes (C_7–C_{40}) analyzed under identical chromatographic conditions. The experimental RI values were then compared with those reported in the literature for the same or equivalent stationary phases, and only compounds with experimental RI values within ± 20 units of the literature values were accepted as confirmed identifications. Due to the unavailability of authentic reference standards, the identifications presented in this study were based on the combined evidence of high-quality mass spectral matching and retention index data, following the recommended practices for GC-MS identification of essential oil components without commercial standards. Relative abundances were measured using peak area normalization without correction factors.

Molecular docking study: Molecular docking was performed to investigate the binding interactions between the major bioactive compounds of CEO (eugenol and eugenyl acetate) and two key membrane-bound enzymes in *F. oxysporum*, namely ERG3 and CYP51, both of which play important roles in fungal survival and pathogenicity. 3D structures of ERG3 and CYP51 were predicted by homology modeling using sequences from the NCBI GenBank database under accession numbers [XP_018248270.1] and [XP_018249826.1] [37,38]. Model quality was assessed using pLDDT confidence scores (regions with pLDDT > 90 were used for docking) and PROCHECK Ramachandran plots (>90% residues in favored regions). Proteins were prepared in AutoDock Tools (v1.5.7) by removing water molecules, adding polar hydrogens, and assigning Gasteiger charges. Ligands (eugenol and eugenyl acetate) were retrieved from PubChem (CIDs: [3314] and [7136]), energy-minimized using the Universal Force Field with 1000 steepest descent steps in Open Babel (v3.1.1), and converted to Protein Data Bank, Partial Charge (Q), and Atom Type (T) (PDBQT) format. Docking simulations were performed using AutoDock Vina (v1.2.5). The grid box (spacing 0.375 Å) was centered at the predicted active site with dimensions of 22 × 22 × 22 Å and coordinates (−10.5, 12.3, 8.7) for ERG3 and (−5.2, 8.1, 15.4) for CYP51. The exhaustiveness was set to 32, and 10 independent runs were performed per complex. The protocol was validated by redocking the native ligand, with an RMSD < 2.0 Å considered acceptable. The lowest-energy pose for each ligand-target pair was selected. Interactions (hydrogen bonds, hydrophobic contacts, π-π stacking) were visualized using PyMOL (v2.5).

Statistical analysis: All statistical analyses were based on the means of biological replicates. The number of biological replicates (n) is indicated in each figure legend or result section. Data were analyzed using SPSS 19.0 (IBM, USA) and GraphPad Prism 9.5 (GraphPad Software, USA) as mean ± standard deviation (SD). Prior to performing one-way ANOVA, the underlying statistical assumptions were verified. Normality of the data was assessed using the Shapiro–Wilk test ($p > 0.05$ indicating a normal distribution), and homogeneity of variances was evaluated using Levene's test ($p > 0.05$ indicating equal variances). All experimental data met these assumptions, confirming the appropriateness of ANOVA for group comparisons. Group comparisons were performed by one-way ANOVA followed by Tukey's post-hoc test ($\alpha = 0.05$) for multiple comparisons. This test was applied to compare mycelial radial growth inhibition, spore germination rates, and ergosterol contents among different CEO concentration groups. Probit regression was used to estimate the EC_{50}, 95% confidence intervals (CI), and concentration-response coefficients based on the pooled data from three independent experiments. Statistical significance was set at $p < 0.05$.

3 Results

Antifungal activity of CEO: In this investigation, CEO demonstrated a dose-dependent inhibition of radial growth *in vitro* (Fig. 1). The inhibitory percentages of CEO against *F. oxysporum* hyphae at concentrations of 50, 100, 150, 200, 250, and 300 μL/L were 16.6%, 35.5%, 51.3%, 69.0%, 77.5%, and 100.0%, respectively (Table 1). Notably, complete suppression was achieved at 300 μL/L ($p < 0.05$).

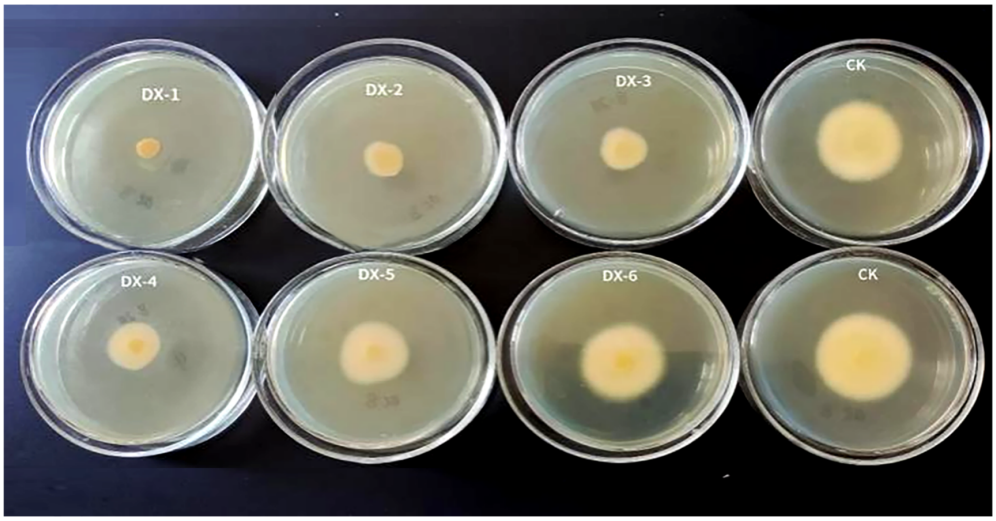

Figure 1: CEO inhibitory effect on *F. oxysporum* mycelial growth. Fungal cultures were treated with CEO at concentrations of 0 (CK, control), 50 (DX-6), 100 (DX-5), 150 (DX-4), 200 (DX-3), 250 (DX-2), and 300 (DX-1) μL/L. Plates were incubated at 28°C for 5 days. Representative images from three independent replicates are shown.

Table 1: Concentration-dependent inhibition of *F. oxysporum* radial growth by CEO.

Treatment Group	CEO Concentration (μL/L)	Radial Growth (mm)	Inhibition Rate (%)
DX-1	300	0.0 ± 0.00f	100.0 ± 0.00a
DX-2	250	6.8 ± 0.39e	77.5 ± 1.85b
DX-3	200	9.3 ± 1.20e	69.0 ± 4.18b
DX-4	150	14.6 ± 1.13d	51.3 ± 7.60c
DX-5	100	19.4 ± 1.36c	35.5 ± 5.86d
DX-6	50	25.1 ± 1.59b	16.6 ± 4.52e
CK	0	30.2 ± 3.31a	0.0 ± 0.00f

Data are mean ± SD of three biological replicates. Means in column marked with different lowercase letters differ significantly ($p < 0.05$) using Tukey's multiple range test. CK represents the untreated control.

In addition, the concentration–response analysis showed a concentration dependent inhibition effect with an EC_{50} of 131.7 μL/L (95% CI: 119.24–149.09), indicating significant antifungal activity (Table 2). These was a better fit ($R^2 = 0.985$) between CEO concentration and the inhibition rate of mycelial cells (Table 2), which shows a reliable dose-response relationship.

Table 2: Probit regression parameters for the inhibitory effect of CEO against *F. oxysporum*.

Essential Oil	Regression Equation (Probit Model)	EC_{50} (μL/L)	95% CI	R^2
CEO	Probit = $2.4736 \times \log_{10}(\text{concentration}) - 0.2428$	131.7	119.24–149.09	0.985

Note: EC_{50} values were calculated by solving the probit regression equation for Probit = 5. The 95% CI were obtained from SPSS probit analysis. Concentration is expressed in μL/L.

Inhibition of F. oxysporum spore germination and morphological change: The CEO induced morphological changes in germinated spores that were directly related to inhibition of germination. The spore germination inhibition test showed that CEO inhibited germination in a dose dependent manner ($p < 0.05$). The inhibition rate significantly increased from 25.1 ± 5.12% at 100 µL/L to 44.8 ± 5.01% at 200 µL/L and 61.6 ± 8.05% at 300 µL/L (Fig. 2I). The germination rate decreased sharply from 72.4 ± 11.51% in the control group to 53.9 ± 5.17%, 39.6 ± 3.13% and 27.3 ± 4.05% in the same treatments, respectively. Statistically, the highest inhibition occurred at CEO concentrations above 200 µL/L.

Microscopic analysis gave an insight into the antifungal mechanism (Fig. 2II). Untreated spores showed long germ tubes and vigorous growth. Exposure to 100 µL/L CEO resulted in growth partially similar to the control, but with a marked decrease in germination frequency. Higher concentrations (200–300 µL/L) led to stronger inhibition: most spores did not germinate, maintained a spherical shape without elongated tubes, and those that did germinate had significantly shorter germ tubes.

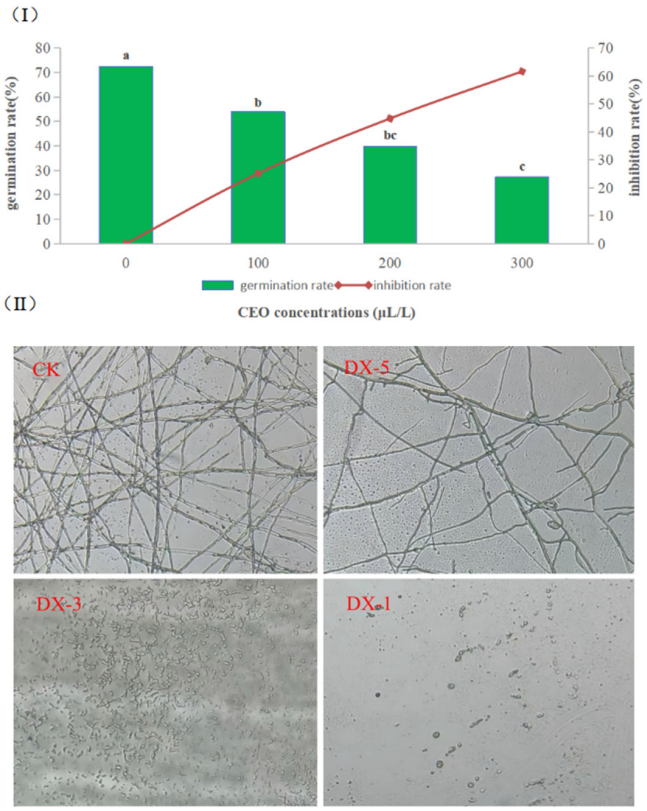

Figure 2: Quantified the inhibition of *F. oxysporum* spore germination by CEO (**I**) and corresponding microscopic. observations across concentrations (**II**). The results display germination rates (green bars), inhibition rates (red line), and representative micrographs of spores treated with CEO at 0 (CK), 100 (DX-5), 200 (DX-3), and 300 (DX-1) µL/L. Data are presented as mean ± SD (n = 3). Lowercase letters indicate significant differences between treatments ($p < 0.05$, Tukey's test); shared letters indicate no significant difference.

CEO inhibits ergosterol biosynthesis: The ergosterol content of *F. oxysporum*, which is essential for maintaining fungal membrane integrity and function, was measured to assess the inhibition of ergosterol biosynthesis by CEO. The inhibition rates for ergosterol biosynthesis were 19.3 ± 1.16%, 24.5 ± 3.14%, and 34.6 ± 0.44% following treatment with CEO concentrations of 50, 100, and 150 µL/L, respectively ($p < 0.05$,

n = 3, Tukey test, Fig. 3). Compared with the untreated control group, this dose-dependent inhibitory effect was more significant at a dose of 150 μL/L.

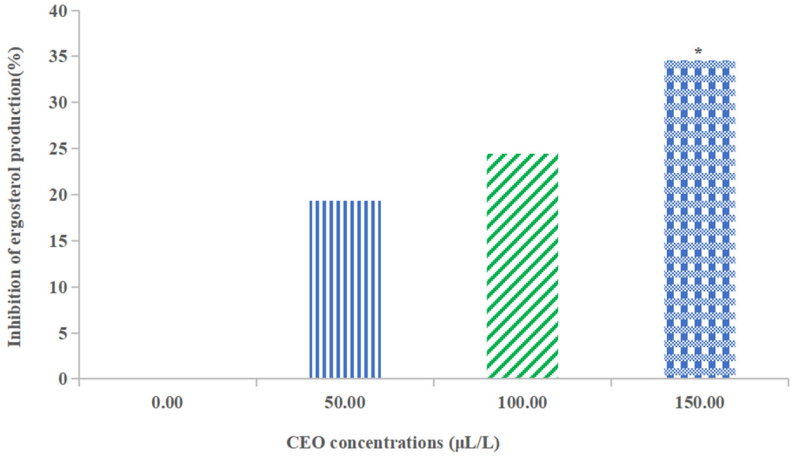

Figure 3: Effects of CEO on ergosterol synthesis in *F. oxysporum*. Dose-dependent inhibition is observed which reached statistical significance at above 150 μL/L compared with control (*$p < 0.05$).

Chemical composition of CEO: CEO was extracted from clove buds by water distillation, and the extraction rate reached 8.3%. Chemical analysis via GC-MS identified 24 volatile compounds in CEO (Fig. 4A), comprising 19 major components that account for 99.32% of the total CEO across seven classes (Fig. 4B). The predominant components were phenylpropanoids (92.44%) with eugenol (72.51%) and eugenyl acetate (19.66%) being the main constituents (Fig. 4C). Based on this composition, molecular docking studies will be performed to the interactions between eugenol and eugenyl acetate with target enzymes involved in the ergosterol biosynthesis.

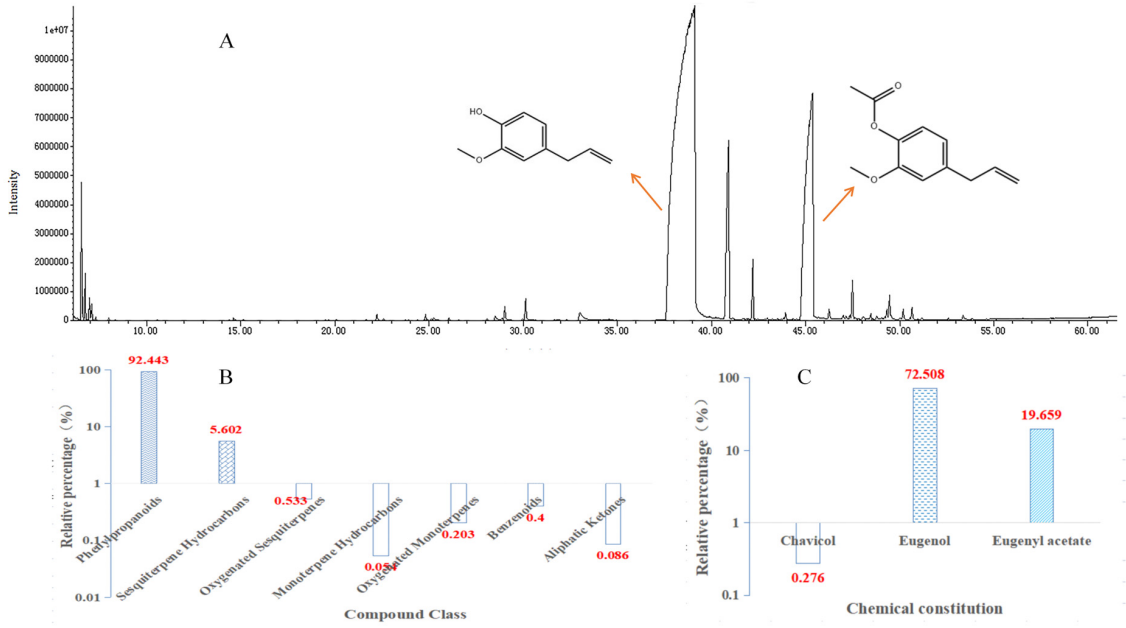

Figure 4: GC-MS analysis of CEO revealed the total ion chromatogram (**A**), the distribution of compound classes (**B**), and the percentages of phenylpropanoid constituents (**C**).

Molecular docking outcomes: Eugenyl acetate demonstrated strong binding energies of −6.615 Kcal/mol for ERG3 and −6.336 Kcal/mol for CYP51. In contrast, eugenol showed weak binding affinity and lower stability, which hinder reliable visualization (Table 3). Fig. 5 shows the 3D binding of eugenyl acetate to both targets. These findings are consistent with the observed *in vitro* antifungal effects and the inhibition of ergosterol synthesis.

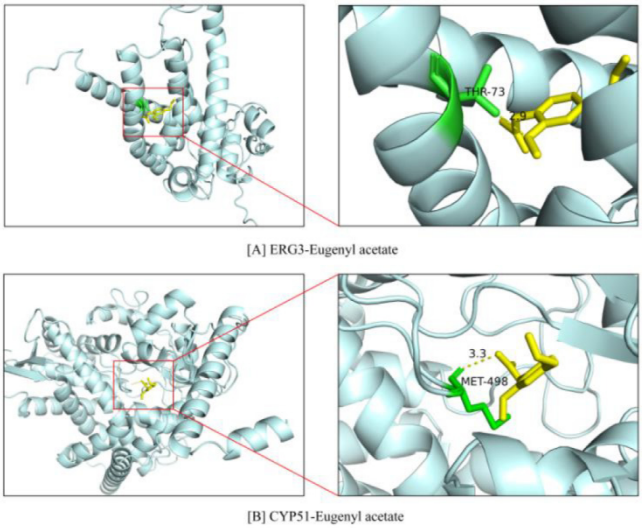

Figure 5: Docked diagram of eugenyl acetate of ERG3 and CYP51. [**A**]: ERG3-eugenyl acetate; [**B**]: CPY51-eugenyl acetate.

Table 3: Top 9 binding free energies of acetyleugenol and eugenol with CYP51 and ERG3.

Target Proteins	Mode	Eugenyl Acetate			Eugenol		
		Affinity (kcal/mol)	Dist from rmsd l.b.	Best Mode rmsd l.b.	Affinity (kcal/mol)	Dist from rmsd l.b.	Best Mode rmsd l.b.
ERG3	1	−6.615	0	0	−5.86	0	0
	2	−6.327	3.159	4.748	−5.712	1.617	2.685
	3	−6.216	3.992	5.893	−5.646	5.693	7.624
	4	−6.058	10.06	10.89	−5.583	14.25	16.48
	5	−6.014	3.318	5.83	−5.535	2.83	5.306
	6	−5.942	3.666	6.104	−5.524	6.569	7.782
	7	−5.831	10.64	12.02	−5.463	13.73	15.5
	8	−5.677	9.437	11.26	−5.459	3.749	5.802
	9	−5.619	10.37	11.22	−5.386	4.513	6.608
CYP51	1	−6.336	0	0	−5.755	0	0
	2	−6.005	12.79	14.5	−5.703	10.11	11.94
	3	−5.978	2.084	5.089	−5.67	19.24	21.26
	4	−5.891	26.81	28.44	−5.647	9.674	11.54
	5	−5.779	26.62	29.17	−5.612	11.01	13.16
	6	−5.766	2.264	3.864	−5.608	10.83	12.76
	7	−5.726	18.44	21.16	−5.541	7.43	9.605
	8	−5.677	15.23	18.75	−5.457	10.17	11.92
	9	−5.616	1.864	2.622	−5.439	14.37	15.71

4 Discussion

As a volatile substance obtained from clove buds by steam distillation, CEO is well recognized for its antibacterial and antifungal properties [39,40], which was further supported by the findings of this

study. Mycelial growth is a key indicator for evaluating antifungal effects, because it reflects the fungal growth and development. The efficacy of CEO in inhibiting mycelial growth was higher than that of *Artemisia dracunculus* extracts reported previously [41,42], as indicated by its lower EC_{50} value ($p < 0.05$). Furthermore, CEO achieved complete suppression of mycelial growth at a concentration of 300 μL/L. Similarly, its inhibitory effect on spore growth exhibited a marked, dose-dependent increase across the tested concentration range (Fig. 2I). Spore morphology showed dose-dependent changes after CEO treatment. At concentrations exceeding 200 μL/L, the treatment resulted in the loss of polarity and swelling, large truncation of germ tubes (50% of control), and total absence of hyphae branching (Fig. 2II). These changes suggest that critical growth processes are disrupted at the early growth stage. The influx of lipophilic components from the essential oil into the cell membrane disrupts membrane integrity, inhibits ergosterol production, and causes changes in shape by changing membrane fluidity and pore structure [43,44]. The positive correlation between CEO concentration and fungal growth inhibition (assessed by both mycelial growth and spore germination) suggests that CEO may function as a natural fungistatic agent.

Ergosterol is a sterol compound unique to fungi. It is the key target for the antifungal effects of CEO [45,46]. Quantitative analyses showed that CEO treatment significantly inhibited ergosterol biosynthesis in *F. oxysporum*, with reductions of 34.6 ± 0.44% at the highest concentration tested (150 μL/L; $p < 0.05$, Tukey's test; Fig. 3). Significant suppression occurred at the 150 μL/L concentration compared to the control. This suggests that CEO directly targets and inhibits key enzymes (cytochrome P450-dependent CYP51) according to the antifungal drug mechanism [47,48]. CYP51 inhibits lanosterol demethylation, leading to accumulation of toxic methylated sterols, loss of membrane symmetry, and decreased H+-ATPase activity [49]. This inhibition adversely affects growth (EC_{50} = 131.7 μL/L) and spore development (63.6% inhibition at 300 μL/L), thereby indicating a multi-targeted antifungal mechanism. Additionally, CEO diminishes membrane fluidity, permeability, and structural stability, leading to the leakage of contents and disruption of membrane bound enzymes. These biochemical alterations contribute to the observed morphological damage in hyphae and spores, further substantiating the role of ergosterol biosynthesis inhibition in the broad-spectrum antifungal activity of CEO. The correlation with CEO concentration also shows its potential as a natural antifungal agent targeting membrane biosynthesis pathways.

The relatively high efficacy of CEO may be attributed to its high content of phenylpropanoids, particularly eugenol and eugenyl acetate, which are known to possess strong membrane-disrupting properties. Unlike some essential oils whose antifungal activity relies on synergistic effects among multiple components, CEO appears to exert its antifungal action primarily via its two major phenylpropanoid constituents. Eugenyl acetate has strong binding affinity with docking energies of −6.615 Kcal/mol for ERG3 and −6.336 Kcal/mol for CYP51. Combinatorial modeling suggests a dual-target mechanism: eugenyl acetate binds to the heme-binding cavity of CYP51, forms hydrogen bonds with Met 498, and interacts with Thr 73 in ERG3. Although it is not sterically inhibited, eugenyl acetate may be hydrolyzed intracellularly to eugenol or may modulate sterol C14-reductase (ERG24) allosterically [50]. The weaker binding affinity and conformal instability limit its binding pose visualization. Only the 3D interactions of eugenyl acetate with both enzyme targets are presented in Fig. 5.

The high affinity of eugenyl acetate for ERG3 and CYP51 indicates that it may be the main bioactive compound underlying the antifungal effects of CEO. These results are consistent with experimental data showing inhibition of ergosterol production and fungal growth, allowing molecular explanations of observed effects. Collectively, the effect on ergosterol biosynthesis shows how CEO has antifungal effects on cells and opens the door to future experiments on mutagenesis [51]. These results resemble the reduction in

ergosterol production and fungal proliferation. In this study, our data show that the inhibition of ergosterol biosynthesis is the main mechanism of the high bioactivity of CEO.

Based on multimodal evidence, a four-step inhibition cascade of CEO activity is proposed. Eugenyl acetate may inhibit enzymes involved in ergosterol biosynthesis (CYP51/ERG3), disrupt membrane integrity, and finally complete inhibition of hyphal and spore growth. This cascade includes dose-dependent effects on spores, with a biochemical inhibition of ergosterol biosynthesis reaching 34.6 ± 0.44% at 150 μL/L. Additionally, it demonstrates high-affinity binding to CYP51 and targets membrane integrity (ERG3 = 6.615 kcal/mol). CEO appears to function through direct growth suppression (EC_{50} = 131.7 μL/L) and membrane targeting. Future studies utilizing pure eugenol and eugenyl acetate in comparative bioassays are essential to validate their individual contributions and confirm eugenyl acetate as the primary active compound. Additionally, to translate these findings into practical applications, encapsulation strategies are essential for improving the formulation properties of CEO and enhancing its antifungal efficacy [52,53]. Although our findings indicate that eugenyl acetate is a promising candidate responsible for the antifungal activity of CEO against *F. oxysporum*.

5 Conclusions

This study demonstrates that CEO exhibits potent, concentration-dependent antifungal activity against *F. oxysporum*. CEO not only inhibits both mycelial growth and spore germination but also causes severe morphological damage, along with suppressing ergosterol biosynthesis through interactions with CYP51 and ERG3. Molecular docking further points to eugenyl acetate as a key bioactive component, given its strong binding affinity to both enzymes. A proposed four-step action model suggests that CEO could be a potential bio-fungicide for controlling root rot diseases, pending further validation with pure compounds and field experiments and *in vivo* assays.

Acknowledgement: The authors sincerely thank the Guizhou Provincial Forestry Science and Technology Research Project (Grant No. QLKH [2025] 10) for its financial support for this work. We also gratefully acknowledge Prof. Shaohuan Liu of Guizhou Medical University for his invaluable assistance in the identification of Syzygium aromaticum (clove), as well as the GC-MS analytical team at the Analysis and Testing Institute for their dedicated technical efforts and support.

Funding Statement: This work was supported by the Scientific Research Foundation for Forestry Science and Technology Project of Guizhou Province (Grant No. QLKH [2025] 10).

Author Contributions: Hualin Hu: wrote original draft, project administration, data curation. Caiwei Wang: data curation, methodology. Jian Fan: methodology, formal analysis. Chengmei Wang: investigation. Chunguang Ren: validation, formal analysis. All authors reviewed and approved the final version of the manuscript.

Availability of Data and Materials: The data are contained within the manuscript.

Ethics Approval: Not applicable.

Conflicts of Interest: The authors declare no conflicts of interest.

References

1. Williamson-Benavides BA, Dhingra A. Understanding root rot disease in agricultural crops. Horticulturae. 2021;7(2):33. [CrossRef].
2. Zhou X, Luo C, Li K, Zhu D, Jiang L, Wu L, et al. First report of *Fusarium striatum* causing root rot disease of *Panax notoginseng* in Yunnan, China. Phyton Int J Exp Bot. 2022;91(1):13–20. [CrossRef].

3. Akash Z, Rajput NA, Atiq M, Malik AU. Assessment of synthetic fungicides against wilt of chilli caused by *Fusarium oxysporum* f. sp. capsica. Pak J Agric Sci. 2022;59(3):485–92. [CrossRef].
4. Rhouma A, Hajji-Hedfi L, Bouqellah NA, Khaire PB, Dali S, Bargougui O, et al. Uniting the role of entomopathogenic fungi against *Rhizoctonia solani* JG Kühn, the causal agent of cucumber damping-off and root rot diseases. Phyton Int J Exp Bot. 2024;93(11):2857–81. [CrossRef].
5. Nawaz H, Ali MA, Atif RM, Nawaz A, Abbas A. Incidence of *Fusarium* wilt in major tomato growing areas of Punjab. Pak J Agric Sci. 2021;58(4):1205–13. [CrossRef].
6. Talubnak C, Parinthawong N, Schoonbeek HJ, Jaenaksorn T. Non-pathogenic Pythium induced the resistance in hydroponic lettuce against root rot disease. Chiang Mai J Sci. 2024;51(3):1–12. [CrossRef].
7. Yang Y, Yang X, Zhang Y, Ren Z, Zhong J, Hu Q, et al. First report of *Fusarium cugenangense* causing root rot of tea plants (*Camellia sinensis*) in China. Plant Dis. 2024;108(1):214. [CrossRef].
8. Ye Q, Wang R, Ruan M, Yao Z, Cheng Y, Wan H, et al. Genetic diversity and identification of wilt and root rot pathogens of tomato in China. Plant Dis. 2020;104(6):1715–24. [CrossRef].
9. Liu SS, Guo N, Ma HX, Sun H, Zheng XJ, Shi J. First report of root rot caused by *Bipolaris zeicola* on maize in Hebei Province. Plant Dis. 2021;105(8):2247. [CrossRef].
10. He Y, Chen J, Tang C, Deng Q, Guo L, Cheng Y, et al. Genetic diversity and population structure of *Fusarium commune* causing strawberry root rot in southCentral China. Genes-Basel. 2022;13(5):899. [CrossRef].
11. Buster M, Simpfendorfer S, Guppy C, Sissons M, Harden S, Flavel RJ. Impact of Fusarium crown rot on root system area and links to genetic variation within commercial wheat varieties. Agronomy. 2023;13(12):2955. [CrossRef].
12. Hale B, Brown E, Wijeratne A. An updated assessment of the soybean-Phytophthora sojae pathosystem. Plant Pathol. 2023;72(5):843–60. [CrossRef].
13. Bradley CA, Allen TW, Sisson AJ, Bergstrom GC, Bissonnette KM, Bond J, et al. Soybean yield loss estimates due to diseases in the United States and Ontario, Canada, from 2015 to 2019. Plant Health Prog. 2021;22(4):483–95.
14. Tyler BM. *Phytophthora sojae*: root rot pathogen of soybean and model oomycete. Mol Plant Pathol. 2007;8(1):1–8. [CrossRef].
15. Khudhair M, Obanor F, Kazan K, Gardiner DM, Aitken E, McKay A, et al. Genetic diversity of Australian *Fusarium pseudograminearum* populations causing crown rot in wheat. Eur J Plant Pathol. 2021;159(4):741–53. [CrossRef].
16. Yin Y, Miao J, Shao W, Liu X, Zhao Y, Ma Z. Fungicide resistance: progress in understanding mechanism, monitoring, and management. Phytopathology. 2023;113(4):707–18. [CrossRef].
17. Zhang N, Xu Y, Zhang Q, Zhao L, Zhu Y, Wu Y, et al. Detection of fungicide resistance to fludioxonil and tebuconazole in *Fusarium pseudograminearum*, the causal agent of Fusarium crown rot in wheat. PeerJ. 2023;11:e14705. [CrossRef].
18. Naqvi SAH, Farhan M, Ahmad M, Kiran R, Shahbaz M, Abbas A, et al. Fungicide resistance in Fusarium species: exploring environmental impacts and sustainable management strategies. Arch Microbiol. 2025;207(2):31. [CrossRef].
19. Coleman D, Geisen S, Wall DH. Soil fauna. In: Coleman DC, editor. Occurrence, biodiversity, and roles in ecosystem function. Amsterdam, The Netherlands: Elsevier; 2015; p. 131–59. [CrossRef].
20. Gobbi A, Kyrkou I, Filippi E, Ellegaard-Jensen L, Hansen LH. Seasonal epiphytic microbial dynamics on grapevine leaves under biocontrol and copper fungicide treatments. Sci Rep. 2020;10:681. [CrossRef].
21. Zhang L, Zuo Q, Cai H, Li S, Shen Z, Song T. Fungicides reduce soil microbial diversity, network stability and complexity in wheat fields with different disease resistance. Appl Soil Ecol. 2024;201:105513. [CrossRef].
22. Zhang Z, Li Y, Xu J, Zou H, Guo Y, Mao Y, et al. The G143S mutation in cytochrome b confers high resistance to pyraclostrobin in *Fusarium pseudograminearum*. Pest Manag Sci. 2024;80(10):4941–9. [CrossRef].
23. Khammanee N, Qiu Y, Kungskulniti N, Bignert A, Meng Y, Zhu Z, et al. Presence and health risks of obsolete and emerging pesticides in paddy rice and soil from Thailand and China. Int J Environ Res Public Health. 2020;17(11):3786. [CrossRef].
24. Cao Z, Zheng X, Guan M, Zhang W, Lin X, Zhao X, et al. Cumulative risk assessment of dietary exposure to pesticide residues in brown rice (*Oryza sativa* L.) from the three main rice-growing regions in China during 2016–2020. J Food Qual. 2022;2022:5902540. [CrossRef].

25. Syamsir DR, Tohar N, Ibrahim H, Mohamad Ali NA, Mokhtar M, Sivasothy Y, et al. Essential oil constituents of *Alpinia scabra* and *Alpinia murdochii*, two wild highland species from peninsular Malaysia and their antimicrobial activity. Sains Malays. 2020;49(1):43–8. [CrossRef].
26. Siddique AB, Ahsan H, Shahid M, Aslam B, Nawaz Z, Hussain R, et al. Preparation and Characterization of Essential oil from *Lavandula spica* Plant and its Antimicrobial Activity against *Pseudomonas aeruginosa* and *Staphylococcus aureus*. Microb Pathog. 2025;198:107157. [CrossRef].
27. Lemos GS, Vitoria JS, Fonseca LM, Pires JB, da Silva FT, Siebeneichler TJ, et al. Active food packages for cake conservation: antifungal potential of bean starch biodegradable films with orange peel essential oil. Int J Biol Macromol. 2025;310:143441. [CrossRef].
28. Hu Y, Zhao Y, Mao Z, Yang J, Huang B, Miao J, et al. Inhalation of Acori Tatarinowii Rhizoma essential oil alleviates dyskinesia in Parkinson's disease rats through the regulation of neuroinflammation. J Ethnopharmacol. 2025;348:119705. [CrossRef].
29. Afreen M, Ucak I. Combined effect of herbal essential oil emulsions and chitosan coatings in conserving physicochemical and microbiological quality of fish meatballs. Pak J Agric Sci. 2025;62(1):121–9. [CrossRef].
30. Raza MS, Saeed M, Butt MS, Shahid M. *In vitro* encapsulation characterization of clove oil microencapsulates. Pak J Agric Sci. 2019;56(3):701–7. [CrossRef].
31. Nasiri-Jahrodi A, Shams-Ghahfarokhi M, Asghari Paskiabi F, Razzaghi-Abyaneh M. Unraveling the mechanism of antifungal action of encapsulated eugenol/chitosan nanoparticles against *Aspergillus fumigatus*. J Drug Deliv Sci Technol. 2024;95:105595. [CrossRef].
32. Ismail AM, Elshewy ES, Ali IH, Elbaki Sallam Muhanna NA, Khafagi EY. Encapsulation of clove oil nanoemulsion in chitosan-based nano-composite: *in vitro* and *in vivo* antifungal activity against *Rhizoctonia solani* and *Sclerotium rolfsii*. Phyton Int J Exp Bot. 2024;93(11):2787–811.
33. Sarma N, Begum T, Pandey SK, Gogoi R, Munda S, Lal M. Chemical profiling of leaf essential oil of *Lantana camara* Linn. from north-east India. J Essent Oil Bear Plants. 2020;23(5):1035–41. [CrossRef].
34. Zhou D, Zhu M, Wei XJ, Hu HL, Cheng BX. Isolation, identification and biological characteristics of three fungi from continuous cropping rhizosphere soil of *Pseudostellaria heterophylla*. J Shandong Agric Univ Nat Sci Ed. 2022;53(6):839–44. (In Chinese). [CrossRef].
35. Phuangsri C, Nuntawong N, Niamsup H. Antifungal activity of the essential oil extracted from *Zanthoxylum piperitum* seeds against *Aspergillus flavus*. Chiang Mai J Sci. 2017;44(2):584–94.
36. Dehghan-Nayeria D, Asgarpanah J, Shams-Ghahfarokhi M, Seyedjavadi SS, Saremi G, Eslamifar A, et al. Antifungal activity, mechanistic insights, and combinatorial effects of *Pycnocycla bashagardiana* essential oil against *Aspergillus fumigatus*. S Afr N J Bot. 2025;181:272–80. [CrossRef].
37. Kundu A, Saha S, Walia S, Dutta TK. Antinemic potentiality of chemical constituents of *Eupatorium adenophorum* spreng leaves against *Meloidogyne incognita*. Natl Acad Sci Lett. 2016;39(3):145–9. [CrossRef].
38. Rajasekharan SK, Kim S, Kim JC, Lee J. Nematicidal activity of 5-ioDOIndole against root-knot nematodes. Pestic Biochem Phys. 2020;163:76–83. [CrossRef].
39. Beyaz MO, Yetiman AE, Doğan M, Horzum M. Examining the possibility of producing natural microbicides and antioxidant agents for food and cosmetic uses from the essential oils of *Laurus nobilis* (laurel), *Syzygium* Aromaticum (clove), and *Cinnamomum verum* (cinnamon). Food Biosci. 2025;69:106840. [CrossRef].
40. Khan L, Khaliq G, Ullah E, Abdul-Rahaman A, El-Mogy MM, Kesba HH, et al. Guggul gum and clove essential oil synergistically reduced anthracnose disease and modulated physicochemical changes in tomato during storage. J Stored Prod Res. 2025;114:102713. [CrossRef].
41. Zhao NN, Yang AP, Jiamiguli M, Yan XR. Fungicidal activity of 8 naturally derived essential oils against four fungi and chemical composition of *Artemisia dracunculus* by GC-MS. Chin J Biol Control. 2022;38(5):1261–8.
42. Ma T, He AM, Liao SX, Aierpani A, Fu SN, Guo J, et al. Analysis of the antibacterial activity of juniper essential oil against the *Sphaeropsis sapinea* of *Pinus sylvestris* var. *mongolica*. J Cent South Univ For Technol. 2025;45(7):164–73. (In Chinese). [CrossRef].
43. Lu XX, Zhu YY, Cheng F, Wu T, Maiwulanjiang M. Ajwain essential oil inhibits aflatoxin B1 and ergosterol production in *Aspergillus flavus*: mechanisms and developmental stages-specific effects. Food Biosci. 2024;62:105561. [CrossRef].

44. Singh K, Deepa N, Chauhan S, Tandon S, Verma RS, Singh A. Antifungal action of 1, 8 cineole, a major component of *Eucalyptus globulus* essential oil against *Alternaria tenuissima* via overproduction of reactive oxygen species and downregulation of virulence and ergosterol biosynthetic genes. Ind Crops Prod. 2024;214:118580. [CrossRef].
45. Yu P, Zhou M, Yu D, Zhang Z, Ye S, Yu Y, et al. Targeted regulation of sterol biosynthesis genes according to perturbations in ergosterol biosynthesis in fungi. J Adv Res. 2025;77:341–56. [CrossRef].
46. Zhang K, Wang Q, Zhang N, Yu L, Lin Q, Zhou W. Inhibition effect of 2-ethylhexanol against *Aspergillus flavus* and aflatoxin B1 mainly by disrupting cell membrane and downregulating genes related to ergosterol synthesis and aflatoxins global regulator. Food Chem. 2025;491:145263. [CrossRef].
47. Prajapati J, Goswami D, Dabhi M, Acharya D, Rawal RM. Potential dual inhibition of SE and CYP51 by eugenol conferring inhibition of *Candida albicans*: computationally curated study with experimental validation. Comput Biol Med. 2022;151:106237. [CrossRef].
48. Zhang R, Wang Y, Wu A, Wang J, Zhang J. Strategies of targeting CYP51 for IFIs therapy: emerging prospects, opportunities and challenges. Eur J Med Chem. 2023;259:115658. [CrossRef].
49. Yang SZ, Peng LT. Significance of the plasma membrane H+-ATPase and V-ATPase for growth and pathogenicity in pathogenic fungi. In: Advances in applied microbiology. Amsterdam, The Netherlands: Elsevier; 2023. p. 31–53. [CrossRef].
50. Li Y, Dai M, Zhang Y, Lu L. The sterol C-14 reductase Erg24 is responsible for ergosterol biosynthesis and ion homeostasis in *Aspergillus fumigatus*. Appl Microbiol Biotechnol. 2021;105(3):1253–68. [CrossRef].
51. Elsaman H, Golubtsov E, Brazil S, Ng N, Klugherz I, Martin R, et al. Toxic eburicol accumulation drives the antifungal activity of azoles against *Aspergillus fumigatus*. Nat Commun. 2024;15(1):6312. [CrossRef].
52. Milićević Z, Krnjajić S, Stević M, Ćirković J, Jelušić A, Pucarević M, et al. Encapsulated clove bud essential oil: a new perspective as an eco-friendly biopesticide. Agriculture. 2022;12(3):338. [CrossRef].
53. Zhang Y, Lu J, Cui K, Wang H, Su J, Zhang W, et al. The encapsulation strategies of clove essential oil enhance its delivery effect in food preservation applications. Food Chem. 2025;484:144465. [CrossRef].